

# Spreading of Aqueous Droplets with Common and Superspreading Surfactants. A Molecular Dynamics Study

Panagiotis E. Theodorakis<sup>a</sup>, Edward R. Smith<sup>b</sup>, Erich A. Müller<sup>c</sup>

<sup>a</sup>*Institute of Physics, Polish Academy of Sciences, Al. Lotników 32/46, 02-668 Warsaw, Poland*

<sup>b</sup>*Department of Mechanical and Aerospace Engineering, Brunel University London, Uxbridge, Middlesex UB8 3PH, United Kingdom*

<sup>c</sup>*Department of Chemical Engineering, Imperial College London, Exhibition Road, South Kensington, London SW7 2AZ, United Kingdom*

---

## Abstract

The surfactant-driven spreading of droplets is an essential process in many applications ranging from coating flow technology to enhanced oil recovery. Despite the significant advancement in describing spreading processes in surfactant-laden droplets, including the exciting phenomena of superspreading, many features of the underlying mechanisms require further understanding. Here, we have carried out molecular dynamics simulations of a coarse-grained model with force-field obtained from the Statistical Associating Fluid Theory to study droplets laden with common and superspreading surfactants. We have confirmed the important elements of the superspreading mechanism, *i.e.* the adsorption of surfactant at the contact line (CL) and the fast replenishment of surfactant from the bulk. Through a detailed comparison of a range of droplets with different surfactants, our analysis has indicated that the ability of surfactant to adsorb at the interfaces is the key feature of the superspreading mechanism. To this end, surfactants that tend to form aggregates and have a strong hydrophobic attraction in the aggregated cores prevent the fast replenishment of the interfaces, resulting in reduced spreading ability. We also show that various surfactant properties, such as diffusion and architecture, play a secondary role in the spreading process. Moreover, we discuss various drop properties such as the height, contact angle, and surfactant surface concentration highlighting dif-

ferences between superspreading and common surfactants. We anticipate that our study will provide further insight for applications requiring the control of wetting.

*Keywords:* Molecular Dynamics Simulation, Surfactants, Water Droplets, Spreading, Coarse-grained Models, Statistical Associating Fluid Theory, Superspreading

---

## Introduction

Superspreading of surfactant-laden aqueous droplets is an exciting phenomenon, which has received a great deal of attention over the last six decades [1–6]. It refers to the unexpectedly rapid spreading of aqueous droplets on hydrophobic substrates, due to the presence of surfactant molecules known as superspreaders [7, 8]. This phenomenon is of fundamental importance for diverse applications, such as coating technology, drug and herbicides delivery, and enhanced oil recovery [2, 9–12]. Although the first reports of superspreading date back to over 50 years ago [3], this phenomenon still attracts considerable attention from both theory and experiment [4, 5, 13–20]. While experimental [18–21] and theoretical [13–17, 22] studies have discussed possible mechanisms of the superspreading for surfactant-laden droplets, certain aspects of this phenomenon require further discussion. This includes the distribution of surfactant molecules within the droplet and the role of surfactant aggregation and diffusion in the spreading process. Moreover, simulation studies have thus far only considered a limited selection of superspreading and common surfactants and a broader selection of surfactants would provide more information towards identifying similarities and differences between surfactant behaviour.

The study of spreading phenomena by computer simulation is well justified, given the availability of reliable all-atom [23–26] and coarse-grained (CG) models [27–44] that enable the faithful simulation of these systems. Indeed, simulations of aqueous solutions with surfactants [13, 22, 45–51] have established the connection between the behaviour of surfactants in the bulk and

spreading [52–55], while the superspreading mechanism and the main characteristics of superspreading surfactants have been the focus of recent studies [5, 13–17, 22, 52, 54–56]. Moreover, experiments have elucidated a number of factors that aid or suppress spreading, such as the rate of evaporation [57], humidity [58], pH [59], surfactant structure and concentration [60, 61], surfactant aging effects [62], surfactant mixtures [63, 64], substrate hydrophobicity [1, 58, 65], and temperature [60, 66]. Despite numerous experimental and numerical studies on the superspreading of surfactant-laden droplets, the study of the superspreading mechanism requires access to molecular-level information of the system, which is not accessible to experiment and continuum simulation. Therefore, we employ here large-scale Molecular Dynamics (MD) simulation of a CG model to study the spreading process by using different common and superspreading surfactants (Fig. 1). We perform analysis of various properties highlighting differences and similarities in the spreading process for these surfactants. Our study also highlights the importance of the aggregation tendency of surfactants, which affects the adsorption efficiency of surfactants at the interfaces and is an important component of the superspreading mechanism [14, 15]. Moreover, properties such as surfactant diffusion and architecture, among others, seem to play a lesser role in superspreading.

## Model and methods

In this study, we carried out MD simulations of a CG model to study systems of aqueous droplets laden with either common or superspreading surfactants. We have considered a widely used superspreader (Silwet L77) and a common surfactant (C10E8) as well as different cases by varying the length of the hydrophilic (common and superspreading surfactants) and the hydrophobic parts (common surfactants) of the surfactants (Fig. 1). Our CG model stems from the SAFT- $\gamma$  molecular-based equation of state (EoS), which analytically describes thermophysical data [67, 68]. This model has proven to be particularly suitable to capture the superspreading of surfactant-laden aqueous

droplets [14, 15] and bulk properties of these systems [14, 50, 51, 69–71]. The EoS offers an accurate fit for force-field parameters, due to the close match between the theory and the underlying Hamiltonian of the system. Hence, it is able to reproduce macroscopically observed thermophysical properties and describe accurately fluid–fluid and fluid–solid interactions [49–51, 69, 72–76]. In fact, the SAFT approach derives robust and transferable potentials of effective beads that represent groups of atoms or even whole molecules (*e.g.* water) with the approach being capable of describing heterogeneous chain fluids [74]. Moreover, the interaction parameters are traced to macroscopic properties of the original segments of the associated pure components [72]. Here, an effective bead ‘W’ represents two water molecules ( $H_2O$ ) with mass  $m_W = 0.8179m$  [69], where  $m$  is the reduced unit of mass corresponding to 44.052 amu. Effective beads ‘M’ represent a  $(CH_3)_3 - Si - O_{1/2}$  chemical group with mass,  $m_M = 1.8588m$ , effective beads ‘D’ correspond to  $O_{1/2} - (CH_3)_2 - Si - O_{1/2}$  groups with mass,  $m_D = 1.6833m$ , ‘EO’ to  $-CH_2 - O - CH_2$  (ether) chemical groups with mass,  $m_{EO} = m$ , and  $-CH_2 - CH_2 - CH_2-$  (alkane, CM) groups with mass,  $m_{CM} = 0.9552$ . We make no distinction between terminal methyl groups and the  $CH_2$  groups [51]. The chemical structures of the common and superspreading surfactants considered in our study are illustrated in Fig. 1.

Effective beads interact via the Mie potential, which is described by the following relation:

$$U(r_{ij}) = C\varepsilon_{ij} \left[ \left( \frac{\sigma_{ij}}{r_{ij}} \right)^{\lambda_{ij}^r} - \left( \frac{\sigma_{ij}}{r_{ij}} \right)^{\lambda_{ij}^a} \right], \text{ for } r_{ij} < r_c \quad (1)$$

where

$$C = \left( \frac{\lambda_{ij}^r}{\lambda_{ij}^r - \lambda_{ij}^a} \right) \left( \frac{\lambda_{ij}^r}{\lambda_{ij}^a} \right)^{\left( \frac{\lambda_{ij}^a}{\lambda_{ij}^r - \lambda_{ij}^a} \right)}.$$

The indices  $i$  and  $j$  indicate the bead type (*e.g.*, W, M, *etc.*). Thus,  $\sigma_{ij}$ ,  $\varepsilon_{ij}$ ,  $\lambda_{ij}^r$ , and  $\lambda_{ij}^a$  are parameters of the Mie potential, while  $r_{ij}$  is the distance between any two beads. The values of the Mie potential parameters for different pairs

of beads are summarised in Table 1; the potential cutoff is set to  $r_c = 4.583\sigma$ . In addition,  $\lambda_{ij}^a = 6$ , irrespective of the bead type [77].

Chain molecules are built by tethering subsequent effective beads together using a harmonic potential,

$$V(r_{ij}) = 0.5k(r_{ij} - \sigma_{ij})^2, \quad (2)$$

where values of  $\sigma_{ij}$  are given in Table 1, and  $k = 295.33\varepsilon/\sigma^2$ .  $\sigma$  is the unit of length while  $\varepsilon$  is the energy unit. Moreover, EO effective beads along the chain interact via a harmonic angle potential, of the form,

$$V_\theta(\theta_{ijk}) = 0.5k_\theta(\theta_{ijk} - \theta_0)^2, \quad (3)$$

where  $\theta_{ijk}$  is the angle between three consecutive beads along a chain,  $k_\theta = 4.32\varepsilon/\text{rad}^2$  is a constant indicating the strength of the harmonic interaction (stiffness of the chain), and  $\theta_0 = 2.75$  rad is the equilibrium angle.

The fluid–substrate interactions were taken into account by integrating the solid potential considering wall composed of spherical Mie beads (implicit substrate) resulting in the following expression [78]:

$$U_{sub}(D) = 2\pi\rho C\varepsilon_{ij}\sigma_{ij}^3 \left[ A \left( \frac{\sigma_{ij}}{D} \right)^{\lambda_{ij}^r - 3} - B \left( \frac{\sigma_{ij}}{D} \right)^{\lambda_{ij}^a - 3} \right]. \quad (4)$$

Here,  $D$  is the vertical distance between beads and the substrate,  $A = 1/(\lambda_{ij}^r - 2)(\lambda_{ij}^r - 3)$  and  $B = 1/(\lambda_{ij}^a - 2)(\lambda_{ij}^a - 3)$ .  $C$ ,  $\sigma_{ij}$ ,  $\varepsilon_{ij}$ ,  $\lambda_{ij}^r$ , and  $\lambda_{ij}^a$  have been defined in Eq. 1, and  $\rho$  is the number density, which typically for a paraffinic substrate is  $\rho \approx 1\sigma^{-3}$ . For the substrate potential the cut-off distance is the same as in the case of fluid–fluid interactions. In the case of the substrate–water (SW) interaction, the strength of the interaction is chosen to provide a contact angle of approximately  $60^\circ$ . To achieve this, the value of the parameter  $\varepsilon_{SW} = 1.4\varepsilon$ . The respective values for the substrate  $\sigma_{SS} = \sigma$  and all fluid–solid interactions can be obtained by employing common combining rules [68], namely,  $\sigma_{ij} =$

$(\sigma_{ii} + \sigma_{jj}/2)$ ,  $\lambda_{ij}^r - 3 = \sqrt{(\lambda_{ii}^r - 3)(\lambda_{jj}^r - 3)}$ , and  $\varepsilon_{ij} = (1 - k_{ij})\sqrt{\sigma_{ii}^3 \sigma_{jj}^3 \varepsilon_{ii} \varepsilon_{jj} / \sigma_{ij}^3}$  [68]. Our model has been matched to experimental data at all stages of the method development and the acquired data were compared with experimental results, with the coarse-grained model specifically parameterised to reproduce: the experimental phase behaviour of water and surfactants [14, 15, 50, 51, 69], the spreading behaviour [14, 15], and observed effects of surfactant architecture and bilayer formation [1, 79].

All simulations were performed in the NVT ensemble by using the Nosé-Hoover thermostat as implemented in the HOOMD package [80] based on the MKT equations [81, 82], with an integration time-step of  $\Delta t = 0.005\tau$ , where  $\tau = \sigma(m/\varepsilon)^{1/2}$  is the time unit. The reduced time unit corresponds to 1.4062 ps. While the size of the simulation box and the number of particles remain constant during the simulation, the temperature fluctuates around a predetermined value, which in our case is  $T = 0.6057$  (corresponding to  $25^\circ\text{C}$ ). The simulation box is  $201\sigma$  long in the  $x$  and  $y$  directions guaranteeing that periodic images of the droplet do not interact with each other due to the presence of periodic boundary conditions in these directions. We have also placed two walls in the  $z$  (normal) direction. The bottom wall is implicit and expressed through Eq. 4 that corresponds to an unstructured wall of infinite thickness. The top wall is represented by LJ beads that interact with the rest of the system through a purely repulsive LJ potential. We typically place  $8 \times 10^4$  beads in the simulation box and bring the droplet in an equilibrium position. as follows: Water and surfactant beads are placed close to each other (*e.g.* in an FCC structure as is usually done in MD simulation) and, also, close to the substrate. Then, running the MD simulation will lead to the formation of a spherical droplet, which can attach to the substrate. At this stage, the potential between the surfactants and the substrate is switched off. Hence, this initial configuration roughly corresponds to the equilibrium state of the aqueous droplet on the paraffinic substrate. Once the droplet reaches the equilibrium, we switch on the potential between the surfactants and the substrate and the nonequilibrium spreading

process starts until a new equilibrium state is reached by the system. Typical trajectories to reach the latter equilibrium depend on the type of surfactant and its concentration. Here, we have considered the same concentration for all cases in order to enable the comparison between the different cases of superspreading and nonsuperspreading processes. This concentration is in the superspreading regime and is  $6.3 \times$  Critical Aggregation Concentration of Silwet-L77 [14]. In general, trajectory lengths were in the range  $10^7$  to  $10^8$  MD steps. Trajectory samples were gathered every  $10^4$  MD steps for all cases, which ensures an independent statistical collection of snapshots required for our analysis while guaranteeing the acquisition of adequate number of snapshots for describing nonequilibrium spreading processes.

### Superspreading

In previous work [15], we used CG MD simulation to propose a mechanism for superspreading of surfactant-laden aqueous droplets, based on a detailed molecular-level analysis of adsorption processes that take place in the droplet during spreading. Figure 2 schematically illustrates these processes at three different stages of spreading in the case of an aqueous droplet with superspreading surfactant (Silwet-L77), namely, an initial and an intermediate nonequilibrium stage (Fig. 2a, b respectively) and an equilibrium final stage (Fig. 2c) of a bilayer conformation. The spherical-cap shape of the droplet gradually transforms into the bilayer structure through the expansion of the contact line as shown in Fig. 2. During this transformation, the directions of surfactant adsorption/desorption processes are illustrated by arrows (Fig. 2a, b, c). While a number of different adsorption processes take place during superspreading, two of them are essential to sustain the rapid spreading of the droplet. The first one is the adsorption of surfactant from the liquid–vapour (LV) interface onto the solid–liquid (SL) interface (substrate) at the contact line (CL), which has been previously suggested by continuum modelling [83]. This adsorption of surfactant at the CL results in an increase in the area of SL and LV inter-

faces, which causes a temporary depletion of surfactant at the interfaces. For this reason, the fast repletion of the interfaces with surfactant from the bulk is crucial in order to sustain the rapid spreading of the droplet. As a result, the ability of effectively adsorbing at the interfaces is an essential feature of superspreading surfactants [15]. In the case of the bilayer structure at the final stages of spreading, surfactants between different parts of the droplet continuously exchange. In this case, there is no dominant direction of adsorption and the system is in a dynamic equilibrium. Characteristic snapshots of aqueous droplets laden with Silwet-L77 surfactants as obtained by MD simulation are presented in Fig. 2, where the distribution of surfactant molecules within the droplet and at the interfaces is illustrated. As the droplet spreads towards the final equilibrium bilayer structure, the aggregates from the bulk supply the interfaces with surfactant. In the final stage, aggregates have dissolved and only surfactant monomers appear within the bilayer.

## Results and Discussion

A quantitative assessment of the distribution of water and surfactant molecules within the droplet at different times can be obtained by calculating the density profiles at the cross-section. The cross-section is perpendicular to the substrate and passes through the centre of mass of the droplet. In the case of droplets with Silwet-L77 (superspreading surfactant, Fig. 3), the density profiles of water molecules indicate the absence of water molecules at certain areas inside the droplet, where the hydrophobic cores of surfactant aggregates are present. On the contrary, water molecules are homogeneously distributed along the LV and the SL interfaces, which are initially connected with the water domains within the droplet. As the droplet spreads, the SL and LV interfaces merge at the CL as is illustrated by the water profiles in Fig. 3, which results in the formation of a bilayer. At an intermediate stage of the spreading process, the bulk of the droplet is dominated by the hydrophobic cores of the surfactant, while at the final stage water molecules are distributed homogeneously along the bilayer



and between the surfactants at the SL and LV interfaces. During the spreading process, the fluctuation in the number of water molecules in the droplet is very small (below 1%) and a slight increase in water is observed as surfactants occupy the interfaces of the droplet during the bilayer formation. The density profile of surfactant molecules indicates a distribution of surfactant without large deviations from the average density at all stages of spreading. Finally, the density distribution of surfactant indicates the boundaries of the droplet as the hydrophobic parts are exposed to the air at the LV interface. The spreading of the droplet is symmetric in all directions onto the  $x - y$ -plane as a result of the smooth unstructured substrate.

We now compare these profiles to typical profiles for common surfactants (Fig. 4). For the range of common surfactants considered in this study, only droplets with C12E5 surfactant eventually form a bilayer structure, but the measured spreading exponent for this case is below the range for superspreading behaviour (0.16–1) at about 0.1. In fact, the density profile of water in the case of C12E5 at an intermediate stage of the spreading process shares some similarities with the case of superspreading due to the initial formation of the bilayer. Although the formation of a bilayer always takes place in the case of superspreading (*e.g.* Silwet-L77, T3E3), certain common surfactants (*e.g.* C12E5) can lead to the formation of bilayer as well, as demonstrated by our computer simulations. Hence, the bilayer structure is characteristic of superspreading behaviour, but it is not a necessary condition. A careful comparison of the density profiles between superspreading and common surfactants indicates a larger heterogeneity of surfactant distribution within the droplet in the case of common surfactants, which reveals an aggregation preference that prevents the surfactants from leaving these aggregates and adsorbing at the interfaces. Indeed, in droplets with common surfactants (Fig. 4) the hydrophobic cores of surfactant aggregates can be better distinguished than in droplets with superspreading surfactant, since local density variations from the average density are larger. Below, we will discuss this point in more detail.

Molecular dynamics simulation can provide estimates of the adsorption rates

of surfactant at different parts of the droplet by tracking individual chains, which is an important strength of molecular-level simulation. Considering an average of the adsorption rates in the ensemble of all surfactants by analysing the individual trajectories of each surfactant during the spreading of the droplet we have confirmed the importance of the surfactant adsorption at the LV interface as well as at the SL interface and to a lesser extent to the CL, and from the bulk to the SL and LV interfaces. These adsorption processes are crucial for the formation of bilayer, but spreading rates vary depending on the ability of the surfactant to replenish the LV and SL interfaces, where a temporary depletion of surfactant is observed during droplet spreading. Our conclusions have been corroborated by the density profiles, which show a tendency of surfactants to remain in aggregates for droplets with common surfactants. Indeed, by following the trajectory of each surfactant molecule within the droplet during spreading we can measure the probability of finding surfactants in different parts of the droplet (Table 2). We have confirmed that common surfactants have a higher tendency to remain in the bulk in the form of aggregates, as the density profiles of Fig. 4 might suggest. Our results also indicate that common surfactants exhibit smaller or comparable probabilities of being at the LV interface and smaller probability of being at the SL interface due to the stronger hydrophobic character of the lyophilic part of the surfactant molecules (cf. interactions in Table 1). This also affects the ability of surfactant to adsorb at the CL. Finally, among the common surfactants considered here, the droplet with C12E5 surfactants is able to form the bilayer structure. In this case, we found the smallest probability that surfactants will stay in the bulk of the droplet. Analysis of the overall diffusion of surfactant molecules within the droplets (Fig. 5) has further underlined the importance of adsorption/desorption processes and the aggregation tendency of surfactants in the spreading process. The overall motion of surfactant within the droplet is subdiffusive irrespective of whether the surfactant is a superspreader. While differences between cases are small, our results suggest that both the size (smaller molecules generally tend to diffuse faster), chemistry and molecular architecture may affect the motion of surfactant in the

droplets, but differences are small. Based on this comparison between common and superspreading surfactants we have concluded that the molecular diffusion plays a minor role in the spreading process and the ability of surfactants to replenish the interfaces during spreading is mainly dictated by the aggregation properties of that surfactant.

Fig. 6 illustrates the time evolution of the number of surfactant molecules per area at the SL interface,  $c_{SL}$ , and the LV surface,  $c_{LV}$ .  $c_{SL}$  is increasing at the initial stages of spreading as the interaction between surfactant molecules and the substrates is switched on reaching a constant value when the final dynamic equilibrium is established. In contrast,  $c_{LV}$  decreases at the initial steps and remains constant during the spreading process. In the case of superspreading surfactants, small changes are observed in the values of  $c_{LV}$  and  $c_{SL}$ . At the final equilibrium bilayer stage, the values of  $c_{LV}$  and  $c_{SL}$  remain constant (not shown here). In the case of the LV surface, there is not an additional interaction (*e.g.* the substrate potential) to attract the molecules at the LV surface. As a result, the spreading process leads to an initial depletion of surfactant at the LV surface and a constant supply of surfactant beyond this initial stage. Overall, the values of  $c_{LV}$  and  $c_{SL}$  depend on the molecular architecture. For example, linear surfactants allow for a better packing at the interfaces. In other words, a larger number of molecules are required to cover the interfaces. This is also illustrated as we attempt to compare the density profiles at the SL and LV interfaces of droplets with different surfactants. Fig. 7 illustrates a typical comparison between superspreading (T3E3) and common (C10E8) spreading cases at the initial and final stages of the spreading process. The density of surfactants appears larger in the case of the linear C10E8 surfactant than in the case of the T-shaped T3E3 surfactant, despite the overall considerably smaller size of the latter. While this difference in behaviour is larger at the SL interface, a smaller difference is observed at the LV surface. Considering the density profiles at the LV and SL interfaces for the solvent molecules (Fig. 8), we found that the interfaces of the droplets are dominated by the surfactants and the solvent's density is rather small. The presence of water at the interfaces is smaller in the

case of the C10E8 surfactant due to the closer packing of the molecules. At the LV interface the T3E3 has formed a bilayer, which is dominated at the CL by water, while the rest of the interface is dominated by surfactant at the bilayer.

Fig. 9 illustrates the time dependence of the droplet height for different surfactant cases. The droplet height is measured from the droplet apex to the SL interface. Hence, there is no direct information about the formation of bilayer when measuring the droplet height. However, we know that the formation of bilayer takes place in the case of droplets with Silwet-L77, T3E3, and C12E5 surfactants. The fluctuations in the height for all cases is a consequence of the continuous depletion and refill of the LV interface with surfactant from the bulk. Droplets with surfactants of smaller size tend to have a smaller droplet height. A comparison between the Silwet-L77 and T3E3 also indicates that the height of the bilayer in the case of T3E3 is smaller than in the case of Silwet-L77. The bilayer height of C12E5 surfactant is larger than in the case of Silwet-L77. This is also reflected in the case of the contact angle (Fig. 10), where smaller surfactants lead to smaller contact angles. In order to measure the contact angle, we have used a linear fit for the LV interface at the CL. Clearly, the formation of bilayer at the CL does not allow for a strict interpretation of our measurements and a more accurate way of measuring the contact angle at the CL, based on the droplet curvature [14], is clearly not applicable in this case. Moreover, we do not attempt here to describe the fluctuating contact angle behaviour, which has been considered in a previous study in detail [84]. However, our measurements of the contact angle at the CL are consistent with the fact that smaller surfactants are associated with smaller contact angles.

## Conclusions

In this study, we have discussed various properties of droplets laden with common and superspreading surfactants. Our analysis has confirmed that the ability of surfactant to adsorb at the interfaces is a key feature of the superspreading mechanism. We have also found that a key feature of nonsuperspread-

ing surfactants is their higher tendency towards aggregates formation, which is a result of the stronger lyophilic interactions. Moreover, the surfactant spatial distribution, diffusion and chain architecture play a smaller role in the spreading process. Finally, we have discussed various properties of the droplets, including height, contact angle and surface concentration, in the context of superspreading behaviour of the droplets. These highlight the different behaviour of common and superspreading surfactants. We anticipate that our work will provide further insight into the spreading mechanisms of surfactant-laded droplets and will underline differences between common and superspreading surfactants. This insight will directly benefit applications requiring the control of wetting through a rational chemical and architectural design of surfactants.

### **Acknowledgements**

The authors would like to thank Omar Matar and Richard Craster for valuable discussions and support on the topic of this study from its very initial stage. This project has received funding from the European Union's Horizon 2020 research and innovation programme under the Marie Skłodowska-Curie grant agreement No. 778104. This research was supported in part by PLGrid Infrastructure.

### **References**

#### **References**

- [1] R. M. Hill, Superspreading, *Curr. Opin. Colloid Interface Sci.* 3 (3) (1998) 247–254.
- [2] A. Nikolov, D. Wasan, Superspreading mechanisms: An overview, *Eur. Phys. J.: Spec. Top.* 197 (1) (2011) 325–341.
- [3] E. G. Schwarz, W. G. Reid, Surface active agents - their behavior and industrial use, *Ind. Eng. Chem.* 56 (1964) 26–35.
- [4] J. Venzmer, Superspreading - 20 years of physicochemical research, *Curr. Opin. Colloid Interface Sci.* 16 (4) (2011) 335–343.

- [5] P. E. Theodorakis, E. A. Müller, R. V. Craster, O. K. Matar, Insights into surfactant-assisted superspreading, *Curr. Opin. Colloid Interface Sci.* 19 (2014) 283–289.
- [6] K. S. I. Sankaran, A., S. Soumyadip, N. Grozev, A. L. Yarin, On the nature of the superspreaders, *Adv. Colloid Interface Sci.* 263 (2019) 1–18.
- [7] K. P. Ananthapadmanabhan, E. D. Goddard, P. A. Chandar, A study of the solution, interfacial and wetting properties of silicone surfactants, *Colloids Surf.* 44 (1990) 281–297.
- [8] S. Rifaï, S. Dipak, V. Bergeron, J. Meunier, D. Bonn, Superspreading: Aqueous surfactant drops spreading on hydrophobic surfaces, *Langmuir* 18 (2002) 10486–10488.
- [9] D. Bonn, J. Eggers, J. Indekeu, J. Meunier, E. Rolley, Wetting and spreading, *Reviews of Modern Physics* 81 (2) (2009) 739–805.
- [10] R. V. Craster, O. K. Matar, Dynamics and stability of thin liquid films, *Reviews of Modern Physics* 81 (3) (2009) 1131–1198.
- [11] O. K. Matar, R. V. Craster, Dynamics of surfactant-assisted spreading, *Soft Matter* 5 (2009) 3801–3809.
- [12] M. J. Rosen, J. T. Kunjappu, *Surfactants and Interfacial Phenomena*, 4th Edition, John Wiley & Sons, New Jersey, 2012.
- [13] R. E. Isele-Holder, A. E. Ismail, Atomistic potentials for trisiloxane, alkyl ethoxylate, and perfluoroalkane-based surfactants with tip4p/2005 and application to simulations at the airwater interface, *J. Phys. Chem. B* 118 (31) (2014) 9284–9297.
- [14] P. E. Theodorakis, E. A. Müller, R. V. Craster, O. K. Matar, Modelling the superspreading of surfactant-laden droplets with computer simulation, *Soft Matter* 11 (2015) 9254–9261.
- [15] P. E. Theodorakis, E. A. Müller, R. V. Craster, O. K. Matar, Superspreading: Mechanisms and molecular design, *Langmuir* 31 (2015) 2304–2309.
- [16] A. T. Badra, H. Zahaf, H. Alla, T. Roques-Carmes, A numerical model of superspreading surfactants on hydrophobic surface, *Phys. Fluids* 30 (2018) 092102.
- [17] H.-H. Wei, Marangoni-enhanced capillary wetting in surfactant-driven superspreading, *J. Fluid Mech.* 855 (2018) 181–209.
- [18] N. M. Kovalchuk, A. Trybala, V. Starov, O. Matar, N. Ivanova, Fluoro- vs hydrocarbon surfactants: Why do they differ in wetting performance?, *Adv. Colloid Interface Sci.* 210 (2014) 65–71.

- [19] N. M. Kovalchuk, O. K. Matar, R. V. Craster, V. M. Starov, The effect of adsorption kinetics on the rate of surfactant-enhanced spreading, *Soft Matter* 12 (2016) 1009–1013.
- [20] N. M. Kovalchuk, A. Trybala, O. Arjmandi-Tash, V. Starov, Surfactant-enhanced spreading: Experimental achievements and possible mechanisms, *Adv. Colloid Interface Sci.* 233 (2016) 155–160.
- [21] K. S. Lee, V. M. Starov, T. J. P. Muchatuta, S. I. R. Srikantha, Spreading of trisiloxanes over thin aqueous layers, *Colloid J.* 71 (2009) 365–369.
- [22] R. E. Isele-Holder, B. Berkels, A. E. Ismail, Smoothing of contact lines in spreading droplets by trisiloxane surfactants and its relevance for super-spreading, *Soft Matter* 11 (2015) 4527–4539.
- [23] J. Hautman, K. M. L., Microscopic wetting phenomena, *Phys. Rev. Lett.* 67 (13) (1991) 1763–1766.
- [24] W. Mar, K. M. L., A molecular-dynamics study of n-hexadecane droplets on a hydrophobic surface, *J. Phys.: Condens. Matter* 6 (23A) (1994) A381–A388.
- [25] C. F. Fan, C. T., Wetting of crystalline polymer surfaces: A molecular dynamics simulation, *J. Chem. Phys.* 103 (20) (1995) 9053–9061.
- [26] J. M. D. Lane, M. Chandross, C. D. Lorenz, M. J. Stevens, G. S. Grest, Water penetration of damaged self-assembled monolayers, *Langmuir* 24 (11) (2008) 5734–5739.
- [27] G. Saville, Computer simulation of the liquid-solid-vapour contact angle, *J. Chem. Soc., Faraday Trans. 2* 73 (1977) 1122–1132.
- [28] J. Sikkenk, J. Indekeu, J. van Leeuwen, E. Vossnack, A. Bakker, Simulation of wetting and drying at solid-fluid interfaces on the delft molecular dynamics processor, *J. Stat. Phys.* 52 (1-2) (1988) 23–44.
- [29] M. Nijmeijer, C. Bruin, A. Bakker, J. V. Leeuwen, A visual measurement of contact angles in a molecular-dynamics simulation, *Physica A: Statistical Mechanics and its Applications* 160 (2) (1989) 166 – 180.
- [30] M. J. P. Nijmeijer, C. Bruin, A. F. Bakker, J. M. J. van Leeuwen, Wetting and drying of an inert wall by a fluid in a molecular-dynamics simulation, *Phys. Rev. A* 42 (1990) 6052–6059.
- [31] J. A. Nieminen, T. Ala-Nissila, Dynamics of spreading of small droplets of chainlike molecules on surfaces, *EPL (Europhysics Letters)* 25 (8) (1994) 593.
- [32] J. A. Nieminen, T. Ala-Nissila, Spreading dynamics of polymer microdroplets: A molecular-dynamics study, *Phys. Rev. E* 49 (1994) 4228–4236.

- [33] M. J. de Ruijter, T. D. Blake, J. De Coninck, Dynamic wetting studied by molecular modeling simulations of droplet spreading, *Langmuir* 15 (22) (1999) 7836–7847.
- [34] T. Blake, A. Clarke, J. D. Coninck, M. de Ruijter, M. Voué, Droplet spreading: a microscopic approach, *Colloids and Surfaces A: Physicochemical and Engineering Aspects* 149 (13) (1999) 123 – 130.
- [35] T. Blake, C. Decamps, J. D. Coninck, M. de Ruijter, M. Voué, The dynamics of spreading at the microscopic scale, *Colloids and Surfaces A: Physicochemical and Engineering Aspects* 154 (12) (1999) 5 – 11.
- [36] M. Voué, S. Semal, J. De Coninck, Dynamics of spreading on heterogeneous substrates in a complete wetting regime, *Langmuir* 15 (22) (1999) 7855–7862.
- [37] M. Voué, S. Rovillard, J. De Coninck, M. P. Valignat, A. M. Cazabat, Spreading of liquid mixtures at the microscopic scale: A molecular dynamics study of the surface-induced segregation process, *Langmuir* 16 (3) (2000) 1428–1435.
- [38] M. Voué, J. D. Coninck, Spreading and wetting at the microscopic scale: recent developments and perspectives, *Acta Mater.* 48 (1819) (2000) 4405 – 4417.
- [39] J. D. Coninck, M. J. de Ruijter, M. Voué, Dynamics of wetting, *Current Opin. Colloid Interface Sci.* 6 (1) (2001) 49 – 53.
- [40] M. Lundgren, N. L. Allan, T. Cosgrove, N. George, Wetting of water and water/ethanol droplets on a non-polar surface: A molecular dynamics study., *Langmuir* 18 (26) (2002) 10462–10466.
- [41] M. Lundgren, N. L. Allan, T. Cosgrove, N. George, Molecular dynamics study of wetting of a pillar surface, *Langmuir* 19 (17) (2003) 7127–7129.
- [42] D. R. Heine, G. S. Grest, E. B. Webb, Spreading dynamics of polymer nanodroplets, *Phys. Rev. E* 68 (2003) 061603.
- [43] T. Werder, J. H. Walther, R. L. Jaffe, T. Halicioglu, P. Koumoutsakos, On the water-carbon interaction for use in molecular dynamics simulations of graphite and carbon nanotubes, *J. Phys. Chem.* 107 (6) (2003) 1345–1352.
- [44] S. J. Marrink, H. J. Risselada, S. Yefimov, D. P. Tieleman, A. H. de Vries, The martini force field: coarse grained model for biomolecular simulations, *J. Phys. Chem. B* 111 (2007) 7812–7824.
- [45] M. S. Tomassone, A. Couzis, C. M. Maldarelli, J. R. Banavar, J. Koplik, Molecular dynamics simulation of gaseous-liquid phase transitions of soluble and insoluble surfactants at a fluid interface, *J. Chem. Phys.* 115 (18) (2001) 8634–8642.



- [46] M. S. Tomassone, A. Couzis, C. M. Maldarelli, J. R. Banavar, J. Koplik, Phase transitions of soluble surfactants at a liquid-vapor interface, *Langmuir* 17 (2001) 6037–6040.
- [47] W. Shinoda, R. DeVane, M. L. Klein, Multi-property fitting and parameterization of a coarse grained model for aqueous surfactants, *Molecular Simulation* 33 (1-2) (2007) 27–36.
- [48] W. Shinoda, R. DeVane, M. L. Klein, Coarse-grained molecular modeling of non-ionic surfactant self-assembly, *Soft Matter* 4 (2008) 2454–2462.
- [49] C. Herdes, E. E. Santiso, C. James, J. Eastoe, E. A. Müller, Modelling the interfacial behaviour of dilute light-switching surfactant solutions, *J. Colloid Interface Sci.* 445 (2015) 16–23.
- [50] O. Lobanova, A. Mejia, G. Jackson, E. A. Müller, Soft- $\gamma$  force field for the simulation of molecular fluids 6: Binary and ternary mixtures comprising water, carbon dioxide, and *n*-alkanes, *J. Chem. Thermodyn.* 93 (2016) 320–336.
- [51] O. Lobanova, Development of coarse-grained force fields from a molecular based equation of state for thermodynamic and structural properties of complex fluids, Ph.D. thesis, Imperial College London (2014).
- [52] Y. Shen, A. Couzis, J. Koplik, C. Maldarelli, M. S. Tomassone, Molecular dynamics study of the influence of surfactant structure on surfactant-facilitated spreading of droplets on solid surfaces, *Langmuir* 21 (2005) 12160–12170.
- [53] H.-Y. Kim, Q. Yin, K. A. Fichthorn, Molecular dynamics simulation of nanodroplet spreading enhanced by linear surfactants, *J. Chem. Phys.* 125 (17) (2006) 174708.
- [54] J. D. Halverson, C. Maldarelli, A. Couzis, J. Koplik, Wetting of hydrophobic substrates by nanodroplets of aqueous trisiloxane and alkyl polyethoxylate surfactant solutions, *Chem. Eng. Sci.* 64 (22) (2009) 4657–4667.
- [55] D. Sergi, G. Scocchi, A. Ortona, Coarse-graining MARTINI model for molecular-dynamics simulations of the wetting properties of graphitic surfaces with non-ionic, long-chain, and T-shaped surfactants, *J. Chem. Phys.* 137 (9) (2012) 094904.
- [56] E. Smith, P. E. Theodorakis, R. V. Craster, O. K. Matar, Moving contact lines: Linking molecular dynamics and continuum-scale modeling, *Langmuir* 34 (2018) 12501–12518.
- [57] S. Semenov, A. Trybala, H. Agogo, N. Kovalchuk, F. Ortega, R. G. Rubio, V. M. Starov, M. G. Velarde, Evaporation of droplets of surfactant solutions, *Langmuir* 29 (32) (2013) 10028–36.

- [58] N. A. Ivanova, Z. B. Zhantenova, V. M. Starov, Wetting dynamics of polyoxyethylene alkyl ethers and trisiloxanes in respect of polyoxyethylene chains and properties of substrates, *Colloids Surf., A* 413 (2012) 307–313.
- [59] J. Radulovic, K. Sefiane, M. E. Shanahan, On the effect of pH on spreading of surfactant solutions on hydrophobic surfaces, *J. Colloid Interface Sci.* 332 (2) (2009) 497–504.
- [60] N. Ivanova, V. Starov, R. Rubio, H. Ritacco, N. Hilal, D. Johnson, Critical wetting concentrations of trisiloxane surfactants, *Colloids Surf., A* 354 (1-3) (2010) 143–148.
- [61] T. Svitova, R. M. Hill, Y. Smirnova, A. Stuermer, G. Yakubov, Wetting and interfacial transitions in dilute solutions of trisiloxane surfactants, *Langmuir* 14 (1998) 5023–5031.
- [62] J. Radulovic, K. Sefiane, M. E. R. Shanahan, Ageing of trisiloxane solutions, *Chem. Eng. Sci.* 65 (18) (2010) 5251–5255.
- [63] M. J. Rosen, Y. Wu, Superspreading of trisiloxane surfactant mixtures on hydrophobic surfaces. 1. interfacial adsorption of aqueous trisiloxane surfactant-n-alkyl-pyrrolidinone mixtures on polyethylene, *Langmuir* 17 (2001) 7296–7305.
- [64] M. J. Rosen, Y. Wu, Superspreading of trisiloxane surfactant mixtures on hydrophobic surfaces 2. interaction and spreading of aqueous trisiloxane surfactant-n-alkyl-pyrrolidinone mixtures in contact with polyethylene, *Langmuir* 18 (2002) 2205–2215.
- [65] J. Radulovic, K. Sefiane, M. E. R. Shanahan, Spreading and wetting behaviour of trisiloxanes, *J. Bionic Eng.* 6 (4) (2009) 341–349.
- [66] N. A. Ivanova, V. M. Starov, Wetting of low free energy surfaces by aqueous surfactant solutions, *Curr. Opin. Colloid Interface Sci.* 16 (4) (2011) 285–291.
- [67] V. Papaioannou, T. Lafitte, C. Avendaño, C. S. Adjiman, G. Jackson, E. A. Müller, A. Galindo, Group contribution methodology based on the statistical associating fluid theory for heteronuclear molecules formed from mie segments, *J. Chem. Phys.* 140 (5) (2014) 054107.
- [68] T. Lafitte, A. Apostolakou, C. Avendaño, A. Galindo, C. S. Adjiman, E. A. Müller, G. Jackson, Accurate statistical associating fluid theory for chain molecules formed from mie segments, *J. Chem. Phys.* 139 (2013) 154504.
- [69] O. Lobanova, C. Avendaño, T. Lafitte, E. A. Müller, G. Jackson, SAFT- $\gamma$  force field for the simulation of molecular fluids. 4. a single-site coarse-grained model of water applicable over a wide temperature range., *Mol. Phys.* 113 (2015) 1228–1249.

- [70] S. Rahman, G. B. C. Lobanova, O. Jiménez-Serratos, V. Raptis, E. A. Müller, G. Jackson, C. Avendaño, A. Galindo, Saft- $\gamma$  force field for the simulation of molecular fluids. 5. hetero-group coarse-grained models of linear alkanes and the importance of intramolecular interactions, *J. Phys. Chem. B* 122 (2018) 9161–9177.
- [71] P. Morgado, O. Lobanova, M. E. A., G. Jackson, M. Almeida, E. J. M. Filipe, Saft- $\gamma$  force field for the simulation of molecular fluids: 8. hetero-segmented coarse-grained models of perfluoroalkylalkanes assessed with new vapour–liquid interfacial tension data, *Mol. Phys.* 114 (2016) 2597–2614.
- [72] E. A. Müller, G. Jackson, Force field parameters from the SAFT- $\gamma$  equation of state for use in coarse-grained molecular simulations, *Annu. Rev. Chem. Biomol. Eng.* 5 (2014) 405–427.
- [73] C. Avendaño, T. Lafitte, A. Galindo, C. S. Adjiman, G. Jackson, E. A. Müller, Saft- $\gamma$  force field for the simulation of molecular fluids. 1. a single-site coarse grained model of carbon dioxide, *J. Phys. Chem B* 115 (2011) 11154–11169.
- [74] C. Avendaño, T. Lafitte, A. Galindo, C. S. Adjiman, E. A. Müller, G. Jackson, Saft- $\gamma$  force field for the simulation of molecular fluids: 2. coarse-grained models of greenhouse gases, *J. Phys. Chem B* 117 (2013) 2717–2733.
- [75] G. Jiménez-Serratos, C. Herdes, A. J. Haslam, G. Jackson, E. A. Müller, Group contribution coarse-grained molecular simulations of polystyrene melts and polystyrene solutions in alkanes using the saft- force field, *Macromolecules* 50 (12) (2017) 4840–4853.
- [76] C. Herdes, A. Ervik, A. Mejía, E. Müller, Prediction of the water/oil interfacial tension from molecular simulations using the coarse-grained saft-mie force field, *Fluid Ph. Equilibria* 476 (2017) 9–15.
- [77] N. Ramrattan, C. Avendaño, E. Müller, A. Galindo, A corresponding-states framework for the description of the mie family of intermolecular potentials, *Mol. Phys.* 113 (9-10) (2015) 932–947.
- [78] E. Forte, A. J. Haslam, G. Jackson, E. A. Müller, Effective coarse-grained solid-fluid potentials and their application to model adsorption of fluids on heterogeneous surfaces, *Phys. Chem. Chem. Phys.* 16 (2014) 19165–19180.
- [79] E. Ruckenstein, Effect of short range interactions on spreading, *J. Colloid Interface Sci.* 179 (1996) 136–142.
- [80] J. A. Anderson, C. D. Lorenz, A. Travasset, A general purpose molecular dynamics simulations fully implemented on graphics processing units, *J. Comput. Phys.* 227 (2008) 5342–5359.

- [81] G. Martyna, D. Tobias, M. Klein, Constant pressure molecular dynamics algorithms, *J. Chem. Phys.* 101 (1994) 4177.
- [82] J. Cao, G. Martyna, Adiabatic path integral molecular dynamics methods. ii. algorithms, *J. Chem. Phys.* 104 (1996) 2028.
- [83] G. Karapetsas, R. V. Craster, O. K. Matar, On surfactant-enhanced spreading and superspreading of liquid drops on solid surfaces, *J. Fluid Mech.* 670 (2011) 5–37.
- [84] E. Smith, E. Müller, R. Craster, O. Matar, A langevin model for fluctuating contact angle behaviour parametrised using molecular dynamics, *Soft Matter* 12 (2016) 9604–9615.

Table 1: Reduced molecular parameters of the Mie interaction potential between effective beads.  $\lambda_{ij}^a = 6$  for all cases. The length and the energy unit are  $\sigma = 0.43635$  nm and  $\varepsilon/k_B = 492$  K, respectively. Therefore,  $k_B T/\varepsilon = 0.6057$ , which corresponds to  $25^{\circ}\text{C}$ .

i-j	$\sigma_{ij}[\sigma]$	$\varepsilon_{ij}[\varepsilon/k_B]$	$\lambda_{ij}^r$
W-W	0.8584	0.8129	8.00
W-M	1.0491	0.8132	13.72
W-D	0.9643	0.6311	10.38
W-EO	0.8946	0.9756	11.94
W-CM	0.9292	0.5081	10.75
M-M	1.2398	0.8998	26.00
M-D	1.1550	0.7114	18.83
M-EO	1.0853	0.8262	22.18
M-CM	1.1199	0.7800	19.61
D-D	1.0702	0.5081	13.90
D-EO	1.0004	0.6355	16.21
D-CM	1.0351	0.5953	14.43
EO-EO	0.9307	0.8067	19.00
EO-CM	0.9653	0.7154	16.86
CM-CM	1.0000	0.7000	15.00

Table 2: Probability of surfactant molecules being at different parts of the droplet (SL, LV, CL, BULK) for different surfactants (T3E3, Silwet-L77, C10E3, C10E8, C12E5, C12E6) as indicated. The average over all surfactants during the spreading process is considered for calculating this probability. The values of the probabilities are truncated to the third digit and probabilities add to unity.

	SL	LV	CL	BULK
T3E3	0.372	0.450	0.080	0.257
Silwet-L77	0.377	0.481	0.083	0.224
C10E3	0.345	0.409	0.059	0.304
C10E8	0.287	0.430	0.074	0.355
C12E5	0.332	0.454	0.072	0.285
C12E6	0.323	0.456	0.077	0.297

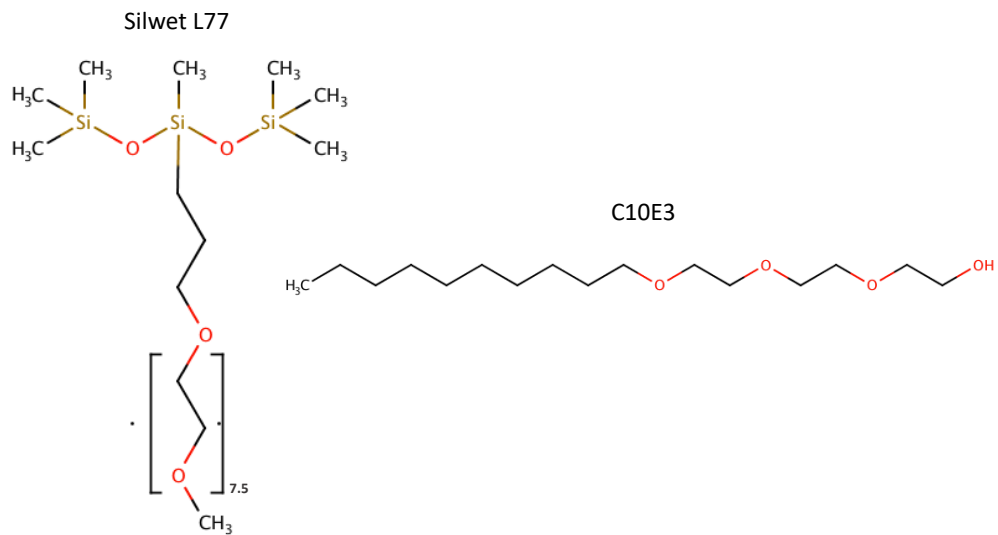


Figure 1: Structure of the superspreading Silwet L77 and common C10E3 surfactants. The T3E3 surfactant has the same structure as the Silwet L77 surfactant, but it only consists of three ethoxyl groups. Similarly the number of alkyl and ethoxyl group are varied accordingly in the case of common surfactants considered in this study, such as C10E8, C12E5, and C12E6.

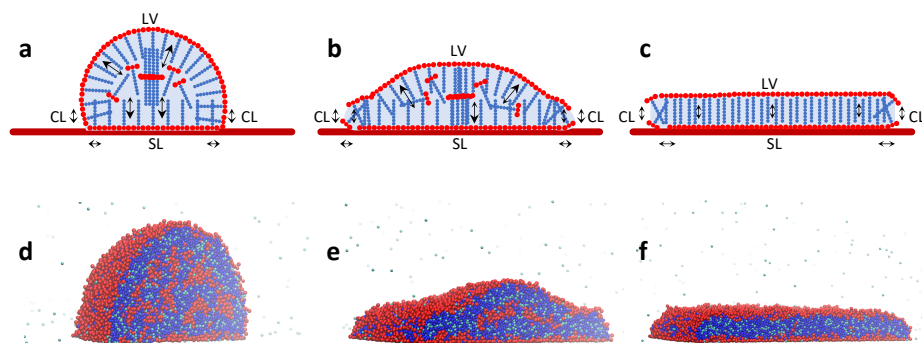


Figure 2: Schematic drawings (a-c) illustrating the dominant directions of adsorption processes during the superspreading of an aqueous droplet laden with Silwet-L77 surfactants and representative snapshots (d-e). ‘LV’ indicates the liquid–vapour interface, ‘SL’ the solid–liquid interface, and ‘CL’ the contact line. In the snapshots, red indicates the hydrophobic groups of the surfactants, while hydrophilic groups are in blue. Water molecules are in cyan. The cross-section of each droplet is shown in order to clearer illustrate the distribution of surfactant within the droplet.

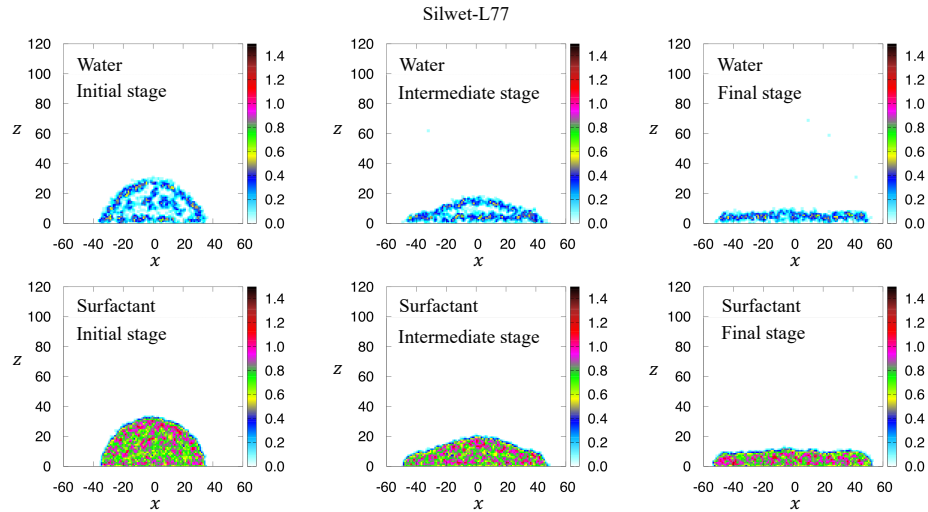


Figure 3: Density profiles of water and surfactant molecules (Silwet-L77) at a cross-section of the droplet (perpendicular to the substrate) at an initial, intermediate, and final stage of superspreading, as indicated. The different colours indicate the density.

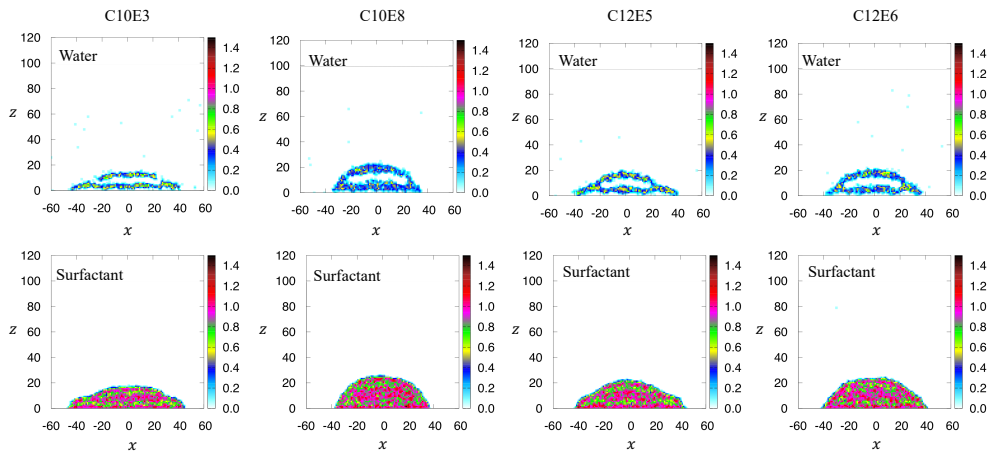


Figure 4: Density profiles of water and surfactant molecules at a cross-section of the droplet (perpendicular to the substrate) for various common surfactants, as indicated. The different colour indicates the density. For the cases of C10E3, C10E8, and C12E6, a representative snapshot of the equilibrium state is shown, whereas in the case of C12E5 a representative snapshot of an intermediate spreading stage is illustrated.

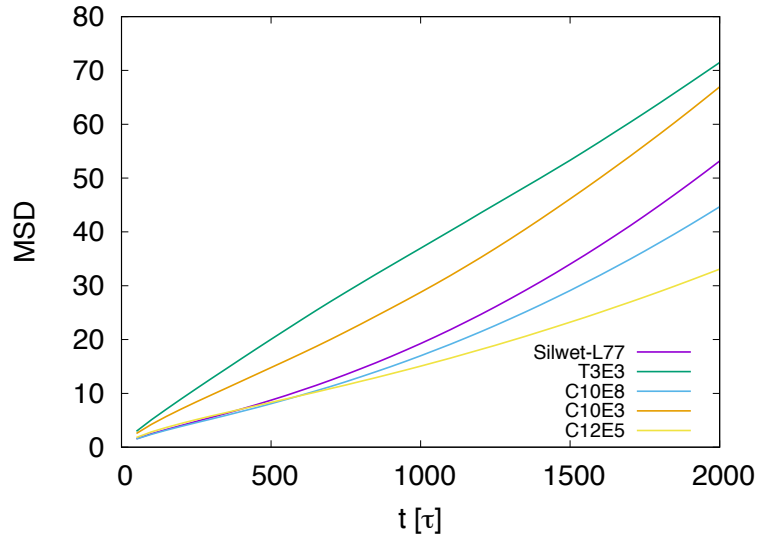


Figure 5: Mean-square displacement for different surfactant as indicated.

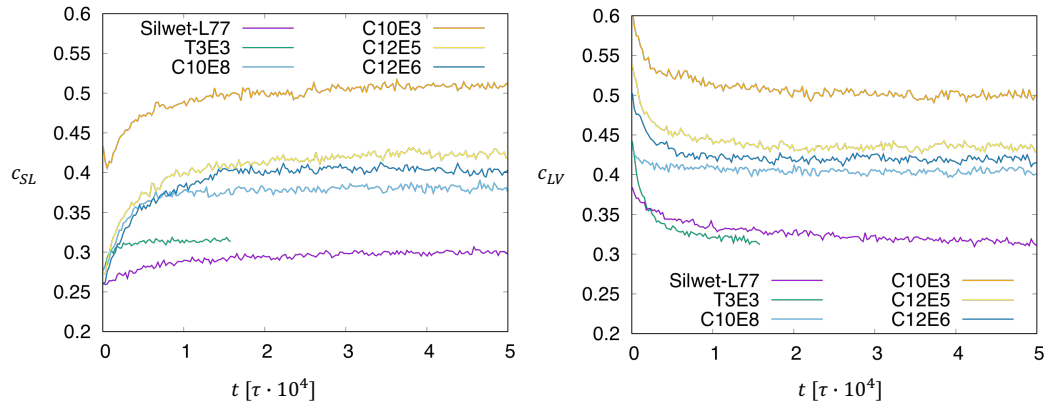


Figure 6: The time evolution of the number of surfactant molecules per area at the SL interface (left panel),  $c_{SL}$ , and the LV surface (right panel),  $c_{LV}$ .



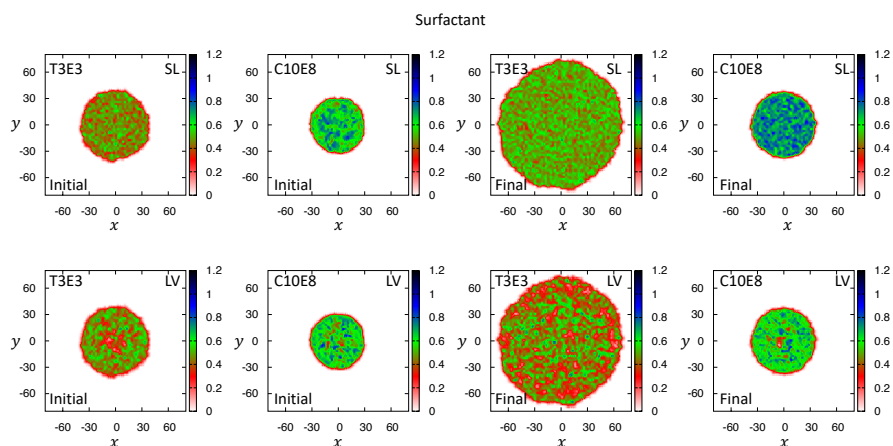


Figure 7: Density profiles of surfactant molecules at the SL interface and the LV surface for two different surfactant cases at an initial and a final stage of spreading as indicated. The different colour indicates the density on the interfaces.

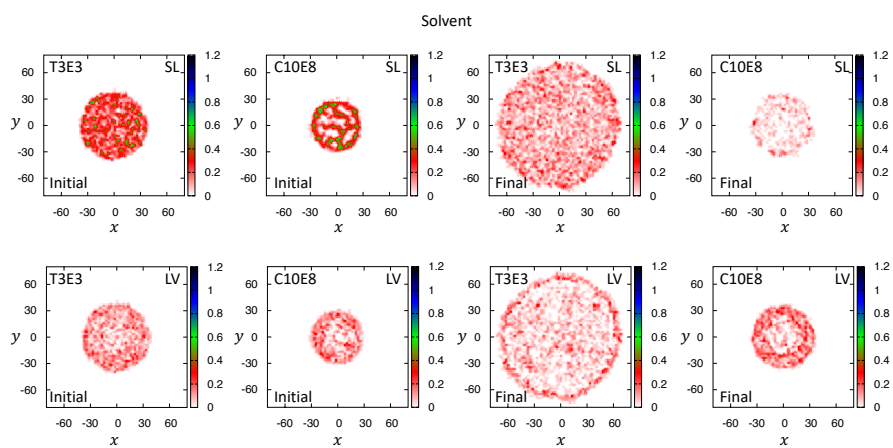


Figure 8: Similar to Fig. 9, but the density of solvent molecules (water) is shown.

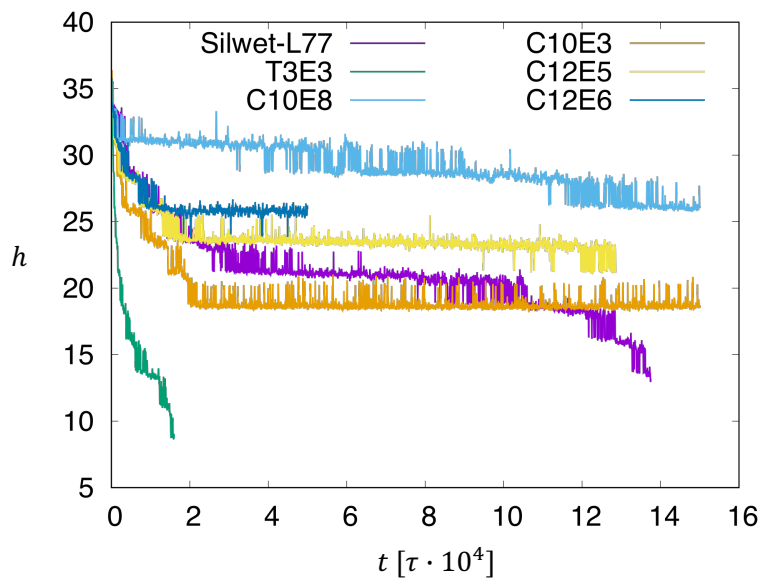


Figure 9: Time evolution of droplet height (measured from the apex to the SL interface) for droplets with different surfactant as indicated.

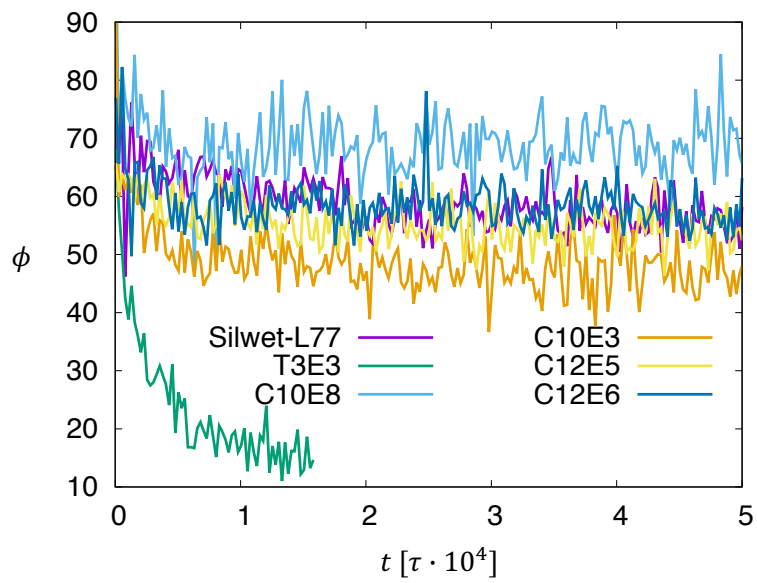


Figure 10: Contact angle  $\phi$  for droplet with different surfactant as indicated.